Frontiers in Bioscience Landmark

Front. Biosci. (Landmark Ed) **2026**; 31(10): 50943
https://doi.org/10.31083/FBL50943

Original Research

Cross-Species Comparison of Diabetic Skin at Single-Cell Resolution: db/db and STZ Mouse Models Versus Human Diabetic Foot Patients

Zhen Xiang[1,2,†], Rui-Peng Cai[1,†], Yun-Feng Chu[3], Yi-Lin Wang[4,5], Zhong Chen[3], Yan-Bin Peng[3,*], Yong-Can Huang[1,*]

[1]Shenzhen Key Laboratory of Spine Surgery, Department of Spine Surgery, Peking University Shenzhen Hospital, 518036 Shenzhen, Guangdong, China
[2]Department of Orthopedics, Shenzhen Xinhua Hospital, 518055 Shenzhen, Guangdong, China
[3]Shenzhen Engineering Laboratory of Orthopaedic Regenerative Technologies, Department of Hand, Foot and Vascular Surgery, Peking University Shenzhen Hospital, 518036 Shenzhen, Guangdong, China
[4]Department of Orthopaedics, Chinese PLA General Hospital, 100853 Beijing, China
[5]National Clinical Research Centre for Orthopaedics, Sports Medicine & Rehabilitation, 100853 Beijing, China
*Correspondence: p1y1b1@163.com (Yan-Bin Peng); y.c.huang@connect.hku.hk (Yong-Can Huang)
[†]These authors contributed equally.
Academic Editor: Graham Pawelec
Submitted: 12 February 2026 Revised: 9 August 2026 Accepted: 31 August 2026 Published: 21 October 2026

Abstract

Background: Research on diabetes-related skin conditions relies primarily on rodent models, including genetic and chemically induced models of diabetes. However, criteria for selecting the most appropriate model remain unclear, and comparative studies at the cellular level are lacking. **Methods:** Full-thickness skin samples were collected from patients with diabetic foot disease, db/db mice, and C57BL/6J mice with streptozotocin (STZ)-induced diabetes. Histological analysis was performed using hematoxylin and eosin staining to assess tissue architecture. Single-cell RNA sequencing (scRNA-seq) was used to characterize cellular composition and transcriptional profiles. **Results:** Human skin was significantly thicker and more stratified than mouse skin. scRNA-seq revealed that human tissue contained a higher proportion of endothelial cells but lacked the adipocyte population observed in STZ-treated mice. Human cells showed greater enrichment in the G1 phase, whereas mouse cells exhibited higher proliferative activity. Transcriptional profiling revealed that human fibroblasts were enriched for markers of chronic inflammation and fibrosis, whereas human keratinocytes and endothelial cells showed increased expression of immune-related genes and decreased expression of metabolic genes. These patterns differed from those observed in the murine models. **Conclusions:** Although the db/db and STZ models reproduce hyperglycemia, they do not fully recapitulate the inflammatory, cell-cycle, and metabolic features observed in human diabetic foot skin. These species-specific differences underscore the need for caution when extrapolating findings from mouse models to human diabetic skin pathology.

Keywords: diabetes mellitus; diabetic foot; single-cell RNA-seq; histology

1. Introduction

Diabetes mellitus (DM) is an increasingly prevalent chronic metabolic disorder characterized by persistent hyperglycemia, which can lead to long-term health complications [1]. There are two primary types of diabetes: type 1 diabetes (T1D) and type 2 diabetes (T2D). T1D arises from the autoimmune destruction of insulin-producing pancreatic β-cells, while T2D is attributed to insulin resistance accompanied by β-cell compensatory failure [2]. Several animal models have been employed to understand the mechanisms underlying DM pathology and to develop new therapeutic strategies, particularly for diabetic wound healing [3].

Currently, T2D is commonly modeled using both obese and non-obese animals, reflecting varying degrees of insulin resistance and β-cell dysfunction [4]. Many studies have investigated diabetic skin conditions, but there is considerable variability in the selection of animal models for laboratory-based diabetes research, with rodent models being the most frequently used [5]. These models primarily fall into two categories: spontaneous and induced diabetes models. Spontaneous models, such as db/db mice and nonobese diabetic (NOD) mice, replicate the pathological features of T2D and T1D, respectively, offering benefits such as genetic stability and natural disease progression [6]. However, these models often progress more slowly and produce lower incidences of certain complications, limiting their application in studies of acute pathology [7]. Conversely, induced diabetes models, such as streptozotocin (STZ)-induced mice and mice given a high-fat diet combined with STZ, use chemical or dietary interventions to induce hyperglycemia rapidly [3]. While these models are advantageous because of their simplicity, low cost, and quick onset of diabetes, their pathological characteristics may differ from those of human diabetes, which often results in poor stability and reproducibility [8]. Currently, no standardized criteria exist for selecting diabetes models, and comparative studies at the cellular level are limited. Iden-

Copyright: © 2026 The Author(s). Published by IMR Press.
This is an open access article under the CC BY 4.0 license.

Publisher's Note: IMR Press stays neutral with regard to jurisdictional claims in published maps and institutional affiliations.

tifying suitable animal models that accurately replicate human diabetic skin and its complications remains a significant challenge.

Single-cell RNA sequencing (scRNA-seq) has revolutionized biological studies by enabling whole-transcriptome amplification at the single-cell level through reverse transcription of mRNA into cDNA, followed by cDNA amplification, and high-throughput sequencing [9]. As an ideal tool for single-cell research, scRNA-seq allows for unbiased, high-throughput analysis with minimal starting material; this helps uncover cell-specific and intercellular differences from the perspective of cellular localization, providing insights into cellular cooperation and tissue heterogeneity [10]. However, few studies have applied scRNA-seq to analyze individual diabetes models or to compare different models. By evaluating single-cell data from various diabetes models, such as STZ-induced and db/db models, researchers can uncover differences in cellular composition, immune response, and angiogenic activity across models, which may help bridge the variant-to-function gap in type 2 diabetes [11]. Furthermore, scRNA-seq can facilitate comparisons of skin tissues from commonly used diabetic mouse models and human diabetic foot patients at both cellular and molecular levels [12]. Such comparisons would deepen our understanding of the similarities and differences between animal models and human patients, clarifying their strengths and limitations and guiding their optimization for the development of personalized therapeutic strategies.

This study thus employed histology and scRNA-seq to compare the skin of db/db mice, STZ-induced diabetic mice, and diabetic patients. Our aim was to provide critical insights, improve experimental methodologies, and offer new evidence for selecting appropriate models for studies on diabetes-related skin conditions.

2. Materials and Methods

2.1 Human Diabetic Skin Collection

The study was approved by the Ethics Committee of Peking University Shenzhen Hospital (No. 2024-122-R2), and all participants provided written informed consent. From March 2024 to June 2025, we recruited subjects with diabetes according to the inclusion and exclusion criteria. The inclusion criteria were as follows: (1) aged between 18 and 80 years; (2) previously diagnosed with diabetes with Wagner classification $\geq$ grade 4; (3) no major surgical procedures within the past month; (4) scheduled for initial debridement or amputation at the surgical site; (5) preoperative completion of relevant imaging studies such as ultrasound and angiography; and (6) consent to participate in the study. The exclusion criteria were as follows: (1) presence of sepsis; (2) concomitant malignancy or autoimmune disease; (3) previous amputation at the surgical site; (4) history of blood transfusion within the past month; (5) receipt of treatments such as growth factors or tissue-engineered skin after admission; and (6) participation in other clinical research projects. Ultimately, five subjects were recruited for enrollment; two were excluded due to insufficient samples for single-cell sequencing, and one withdrew for personal reasons, resulting in two subjects included in the study.

Due to the clinical and surgical needs of the enrolled subjects, removal of the diseased limb segment was performed during surgery. Thus, debridement and amputation samples from diabetic foot subjects were collected as surgical waste during routine clinical procedures, posing no additional risk to the participants. After removal, the samples were rinsed with sterile saline, and full-thickness skin was excised with a scalpel and divided into portions. These samples were placed in 15 mL sterile centrifuge tubes and tissue culture tubes for further analysis. Portions of each sample were sent for hematoxylin and eosin (HE) staining and single-cell transcriptome sequencing, and the remaining samples were stored short-term at 4 °C. The leftover tissue was processed according to hospital regulations. Relevant clinical data, including basic patient information, imaging, and routine blood tests, were retained.

2.2 Skin Collection From db/db Mice and STZ Mice

This study was approved by the Ethics Committee of Peking University Shenzhen Hospital (No. PKUSZH-Ethics-Research-2024-105). Five-week-old male C57BL/6J mice (n = 10) were selected and acclimated for one week; nine-week-old db/db mice (n = 5) were also selected and acclimated for one week for subsequent experiments. The animals were purchased from Jiangsu Hua-chuangSino Pharma Tech (Jiangsu, China).

Six-week-old male C57BL/6J mice (n = 10) were fasted for 12 h and then given a single intraperitoneal injection of STZ (Cat. No. S8050, Lot No. 2230815002, purchased from Solarbio, Beijing, China) at a dose of 150 mg/kg. Blood glucose levels were measured on days 3, 7, and 14 post-injection, along with body weight recordings. Two C57BL/6J mice died within 3 days post-injection, and one exhibited blood glucose levels below 16.7 mmol/L on day 3. The remaining 7 C57BL/6J mice maintained blood glucose levels $\geq$16.7 mmol/L across all three measurements, confirming successful model induction. These six-week-old male C57BL/6J mice averaged approximately 17 g in body weight at the time of injection. After STZ injection, the mice exhibited a rapid decline in body weight within the first week, gradually slowing to stabilize at an average of 14 g by 10 weeks of age. After the STZ-induced diabetic mice were anesthetized with isoflurane gas, a circular full-thickness wound (approximately 1.0 cm in diameter) was created on the dorsal skin using a punch. Full-thickness skin samples were then collected from each group. Portions of each sample were sent for HE staining and single-cell transcriptome sequencing, and the remainder was stored short-term at 4 °C.

Ten-week-old male db/db mice (n = 5) with blood glucose levels ≥16.7 mmol/L were included. Body weight and fasting blood glucose levels were recorded prior to surgery. All surgical procedures were performed under general anesthesia induced by inhalation of 3%–5% isoflurane and maintained with 1.5%–2.5% isoflurane in oxygen (1 L/min). After anesthesia, a circular full-thickness skin defect with a diameter of 1.0 cm was created at the midline of the back (centered on the costovertebral angle) via a punch. Full-thickness skin samples were collected, with portions sent for HE staining, single-cell transcriptome sequencing, and stored short-term at 4 °C. Outcome assessment and histological/analytical procedures were performed by investigators blinded to group allocation. At the experimental endpoints, the animals were euthanized via an overdose of isoflurane inhalation (5% in a closed chamber) followed by cervical dislocation to ensure death, in accordance with the institutional ethical guidelines, the Animal Research: Reporting of *In Vivo* Experiments guidelines, and the National Institutes of Health Guide for the Care and Use of Laboratory Animals.

2.3 HE Staining

All tissue samples were processed into paraffin sections with a thickness of approximately 4 μm after fixation, dehydration, clearing, and embedding. Sections were baked on a slide warmer to remove excess paraffin, deparaffinized with xylene, and dehydrated sequentially with graded ethanol solutions (70%, 80%, 95%, and 100%). These sections were subsequently stained with hematoxylin to label the nuclei, rinsed with running tap water to remove excess stain, differentiated with acid alcohol, and washed again with water to achieve bluing. Eosin was used to stain the cytoplasm. The sections were dehydrated through graded ethanol, cleared with xylene, and mounted with neutral resin. Finally, the slides were examined and imaged under a microscope for pathological analysis.

2.4 Single-Cell RNA Sequencing

Single-cell RNA sequencing procedures were performed by Beijing Xunyin Biotechnology Co., Ltd (Beijing, China). The concentration and purity of the sequencing samples met the requirements. The process included enzymatic digestion of full-thickness skin samples with trypsin to dissociate them into single-cell suspensions while minimizing cell damage and RNA degradation. Cell count and viability were assessed using a fluorescence cell analyser (Countstar Rigel S2) with AO/PI reagent after erythrocyte removal (Solarbio R1010). Dead cells and debris were removed to improve the quality of downstream sequencing. Single cells were encapsulated with barcoded microbeads in droplets via a microfluidic chip. Within the droplets, cell lysis occurred, releasing RNA captured by barcoded oligonucleotide beads and allowing individual indexing for subsequent data analysis. cDNA was synthesized from the RNA using reverse transcriptase and amplified via PCR to obtain a sufficient template. cDNA fragments were enzymatically digested to a suitable size for sequencing (200–500 bp), and sequencing adapters containing sequencing primer binding sites and cell barcodes were ligated to both ends. Libraries were purified with magnetic beads to remove unligated adapters and small fragments, and their quality and concentration were assessed via qPCR. The final libraries were sequenced on Illumina NovaSeq 6000 with a PE150 read length mode (Reagent Kit Version v1.5, Manufacturer Illumina, Inc., San Diego, CA, USA).

Post-sequencing, the raw data underwent several bioinformatics analyses: (1) Data preprocessing: This involved filtering to remove low-quality reads and those with adapter contamination. The remaining reads were aligned to the reference genome (e.g., human genome GRCh38). PCR duplicates were eliminated based on cell barcodes and unique molecular identifiers (UMIs). (2) Gene expression quantification: The expression levels of each gene in each cell were calculated to generate a gene expression matrix. (3) Dimensionality reduction and clustering: High-dimensional data were reduced using UMAP (Uniform Manifold Approximation and Projection) for clustering to identify different cell types or subpopulations. (4) Differential expression analysis: Gene expression differences between distinct cell groups were analyzed to identify specific marker genes. (5) Trajectory inference: Pseudotime analysis methods reconstructed developmental trajectories or state transitions of cells. (6) Functional enrichment analysis: Differentially expressed genes (DEGs) underwent functional annotation (e.g., GO and KEGG analyses) to explore their biological significance.

2.5 Statistical Methods

Raw single-cell data were assessed using statistical distribution models (e.g., negative binomial distribution) to evaluate sparsity and noise levels in gene expression data, applying statistical thresholds (e.g., number of detected genes per cell, total UMI count, and mitochondrial gene proportion) to filter out low-quality cells. Highly variable genes were identified via variance–mean relationship models, such as the negative binomial-based highly variable gene selection method in Seurat. The main expression features were extracted based on the covariance matrix to reduce data dimensionality; utilizing probabilistic distribution methods were then used to map the high-dimensional data into low-dimensional space while preserving local cell structure. Generalized linear models analyzed DEGs between cell populations, with the Benjamini–Hochberg method applied to control the false discovery rate of the results. The dynamic trajectories of cell states were reconstructed via the minimum spanning tree approach and evaluated through goodness-of-fit measures. Hypergeometric tests assessed the enrichment of DEGs in specific functional categories, with enrichment significance evaluated

using the Kolmogorov–Smirnov test on ranked gene lists. Finally, the batch effects of different samples were eliminated using the Harmony method based on linear mixed models.

3. Results

3.1 Pathological Comparison

As illustrated in Fig. 1, the human epidermis was distinctly stratified, featuring a thick, well-organized stratum corneum, approximately three layers of flattened cells in the granular layer, about ten keratinocytes in the spinous layer, and 1–2 columnar cell layers in the basal layer. The dermis was thicker, containing numerous vessels of varying sizes, and showing marked inflammatory infiltration, while well-structured skin appendages were scarce. In comparison, both db/db and STZ mice exhibited simplified epidermal structures characterized by a loose stratum corneum, roughly one layer of flattened cells with basophilic nuclei, and one–two layers of keratinocytes. The stratum corneum was thinnest and least organized in db/db mice, slightly thicker and denser in STZ mice, yet still thinner than in human patients. db/db mice exhibited a thicker subcutaneous fat layer filled with lipid vacuoles. The overall skin thickness in both mouse models was less than that seen in human patients, with db/db mice having a slightly thicker epidermis but a thinner dermis than STZ mice. Additionally, the dermal vasculature was reduced in both mouse models, with vessel density being slightly higher in STZ than in db/db mice. Notably, skin appendages were abundant in both mouse models—predominantly hair follicles with fewer sebaceous and sweat glands—whereas human patients had very few well-structured appendages. Cell counts indicated epidermal and dermal cell densities of approximately 3500 and 1300 cells per 10^6 μm^2 in human patients, 7400 and 2000 in db/db mice, and 6800 and 1200 in STZ mice, respectively.

3.2 Single-Cell QC Analysis

After the preparation of single-cell suspensions from skin samples of STZ mice, db/db mice, and diabetic foot patients, quality control checks were performed to confirm that the samples met the required standards. Cells expressing fewer than 500 genes or more than 5000, those with mitochondrial content exceeding 10%, and cells with total RNA molecule counts above 30,000 were filtered out. Following this step, 21,226 cells were obtained from the skin specimens of two STZ mice, 23,300 cells from two db/db mice, and 22,344 cells from two diabetic foot patients.

3.3 Cell Subpopulations in the Skins of the Three Groups

We generated expression plots for marker genes and annotated cells in different clusters (Fig. 2A–C). Keratinocytes were identified by the marker genes *KRT1*, *KRT5*, and *KRT14*; fibroblasts by *DCN*, *LUM*, *COL1A1*, and *COL1A2*; endothelial cells by *SELE*, *PECAM1*, *CDH5*, and *VWF*; vascular smooth muscle cells/pericytes by *TAGLN*, *ACTA2*, *RGS5*, and *PDGFRB*; myeloid cells by *CD14*, *IL1B*, and *LYZ*; melanocytes by *MLANA*, *PMEL*, *TYRP1*, and *DCT*; Schwann cells by *NRXN1*; sweat gland cells by *AQP5*; T cells by *CD3D* and *CD3E*; B cells by *CD19*, *CD79A*, and *MS4A1*; and adipocytes by *ADIPOQ* and *FABP4*. The primary cell types in the skin of all three groups included keratinocytes/basal cells, endothelial cells, vascular smooth muscle cells/pericytes, fibroblasts, myeloid cells, melanocytes, Schwann cells, sweat gland cells, T cells, and B cells. Keratinocytes and fibroblasts were significant components of the skin of STZ mice, db/db mice, and diabetic foot patients. However, the proportions of endothelial cells and vascular smooth muscle cells/pericytes were higher in diabetic foot patients than in the two diabetic mouse models. Sweat gland cells were present in the skin of diabetic foot patients but were rarely found in STZ and db/db mice. Conversely, adipocytes were observed in the skin of STZ mice but were nearly absent in db/db mice and diabetic foot patients. Furthermore, we performed dimensionality reduction and clustering on a subset of marker genes (Fig. 2D).

3.4 Cycle Analysis

Cell cycle analysis revealed that approximately 76% of the cells in the skin of diabetic foot patients were in the G1 phase, whereas 24% were in the G2M or S phase. In db/db mice, about 60% of the cells were in G1, and 40% were in G2M or S. In STZ mice, approximately 45% of the cells were in G1, while 55% were in G2M or S. Diabetic foot patients had the highest proportion of cells in G1 phase, while STZ mice had the highest proportion in G2M or S phase (Fig. 2E).

3.5 Cell–Cell Interaction Analysis

In the skin of db/db mice, STZ mice, and diabetic foot patients, common pairs of cell types exhibited strong interactions: fibroblasts and keratinocytes, with the primary ligand–receptor pair being COL1A1/COL1A2–ITGA1+ITGB1; fibroblasts and endothelial cells, with the core ligand–receptor pairs including PDGFA–PDGFRA and FGF2–FGFR1; and endothelial cells and keratinocytes, with the core ligand–receptor pairs comprising ANGPT2–TEK and VEGFA–VEGFR2. Notably, diabetic foot patients displayed relatively stronger interactions involving inflammatory cells, specifically HLA–DRA–CD4 and CCL5–ACKR1, while KITL–KIT signaling between melanocytes and keratinocytes was absent. By contrast, STZ mice showed that adipocytes were more actively involved in intercellular interactions, chiefly through ligand–receptor pairs such as ADIPOQ–ADIPOR1, ADIPOQ–ADIPOR2, LEP–LEPR, and CSF1–CSF1R (Fig. 3). This analysis confirmed that fibroblasts and keratinocytes closely interacted with other cell types across all three groups. Compared with STZ

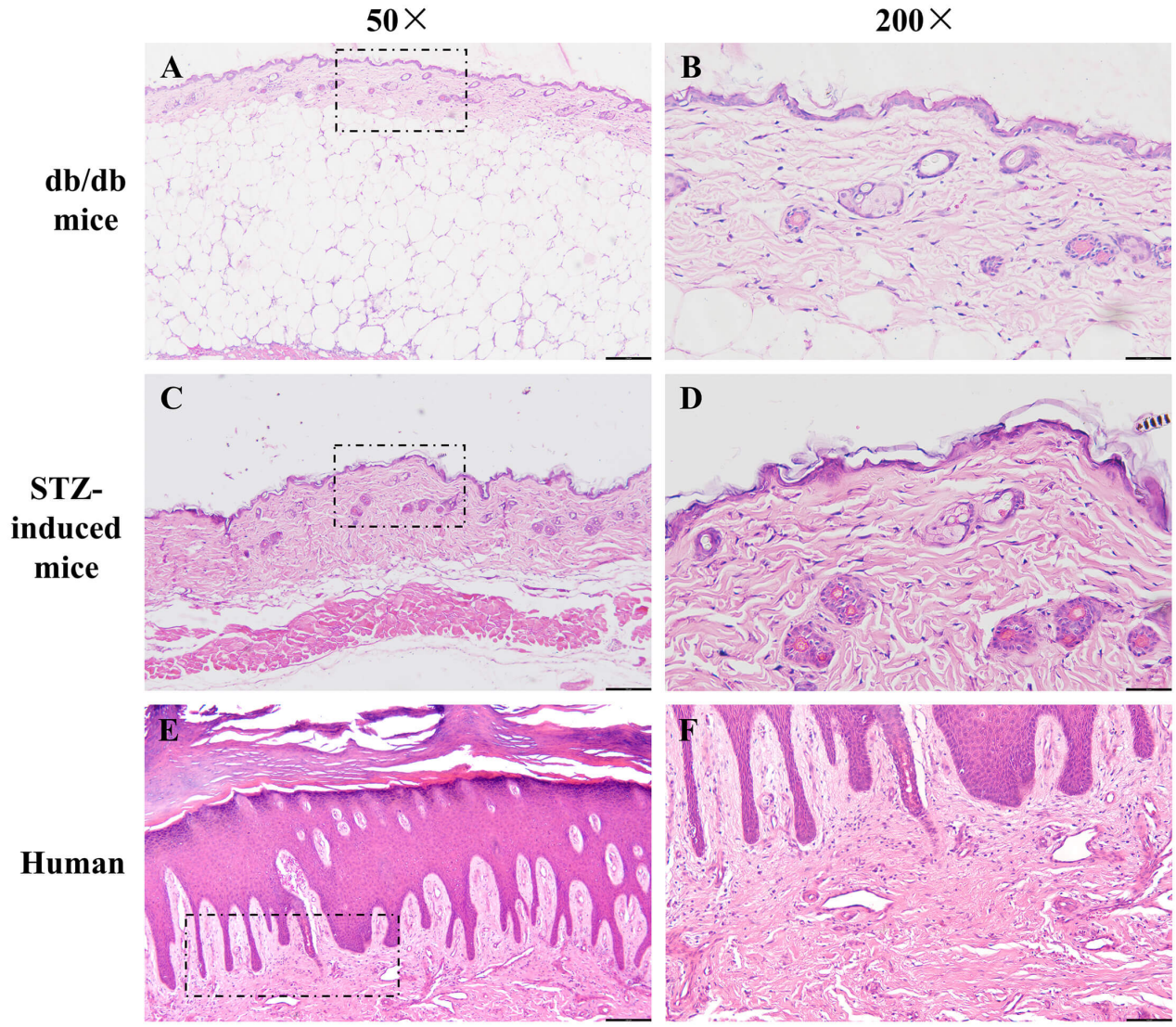


Fig. 1. Histological comparison of skin from db/db mice, STZ mice, and DF patients. Left panels show low-magnification views (50×) of the overall epidermal and dermal architecture, with dashed boxes indicating the regions enlarged in the corresponding right panels (200×). Scale bars: 200 µm (50× images) and 50 µm (200× images).

mice and db/db mice, the skin of diabetic foot patients exhibited more complex and tighter intercellular interactions, particularly involving endothelial cells, vascular smooth muscle cells/pericytes, and inflammatory cells (Fig. 3A,B).

3.6 Myeloid Cell Differential Analysis

The myeloid cell population in the skin of the three groups consists of monocytes, macrophages, Langerhans cells, and dendritic cells, with macrophage subpopulations comprising the majority (Fig. 4A). In the skin of db/db mice and STZ mice, myeloid cell subpopulation classification was highly similar, divided into seven distinct subclusters: c-1 (monocyte subpopulation) expressed Cd14, S100a8, and S100a9; c-2 (macrophage subpopulation) expressed Hspa1a, Hspa1b, and P2rx7; c-3 (macrophage subpopulation) expressed Rsad2, Ccl4, and Ccl7; c-4 (macrophage subpopulation) expressed Clec4e, Thbs1, Cxcl3, and Il10; c-5 (macrophage subpopulation) expressed Ctsl, Lpl, and Gpnmb; c-6 (Langerhans cell subpopulation) expressed Cd207, Mfge8 and Il1r2, and c-7 (dendritic cell (DC) subpopulation) expressed Ramp3, Timd4, and Cytip. Unlike db/db and STZ mice, whose myeloid subpopulation clustering was highly similar to each other, diabetic foot patients showed more concentrated and better-defined clustering, comprising five distinct subclusters: c-1 (macrophage subpopulation) expressed CTSL, PID1, and SPP1; c-2 (macrophage subpopulation) expressed HSPA6, HSPA1B, and DNAJB1; c-3 (macrophage subpopulation) expressed SERPINB2 and IL1B; c-4 (dendritic cell subpopulation) expressed DAPP1, CCR7, and LAMP3; and c-5 (Langerhans cell subpopulation) expressed HLA-DQB2, TBC1D4, and CD207 (Fig. 4B). Functional enrichment analysis of genes

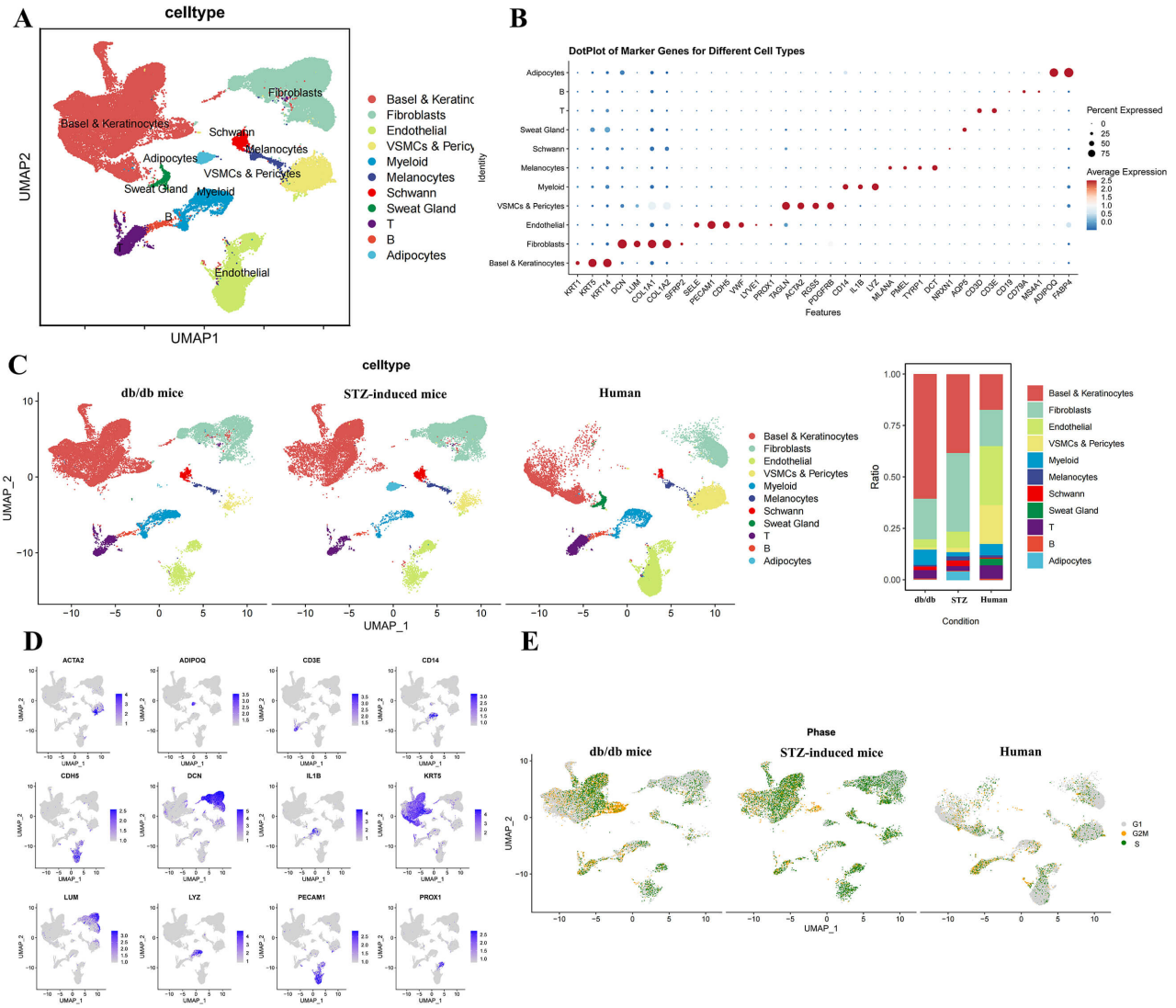


Fig. 2. Overview of single-cell transcriptomes from diabetic mice and human skin. (A) UMAP cell-type distribution shows the clustering results of skin single-cell transcriptomes in UMAP. Each point represents a cell, and the colors correspond to the annotated cell types. (B) The bubble plot shows the expression of representative marker genes across cell types. The bubble size indicates the percentage of cells expressing the gene, and the color of the dots indicates the normalized average expression. (C) UMAP projections, cell-type annotations, and the relative proportions of each cell type are shown separately for the three groups: db/db mice, STZ mice, and human. (D) Marker-subset dimensionality reduction and clustering. (E) In the cell cycle analysis, each dot represents a single cell; different colors denote distinct phases: White indicates the G1 phase, orange indicates the G2 or M phase, and green indicates the S phase. UMAP, Uniform Manifold Approximation and Projection.

from the relatively abundant myeloid subpopulation, c-2, in db/db and STZ mice indicated that this subpopulation likely played a significant role in humoral immunity and antibody-mediated processes (Fig. 4C). In human diabetic foot patients, functional enrichment analysis of the most abundant myeloid subpopulation, c-1, underscored its crucial role in injury repair (Fig. 4D).

3.7 Differential Analysis of Fibroblasts

Fibroblast subpopulation classification in the skin of db/db mice and STZ mice was highly similar, with five distinct subclusters identified: c-1 expresses Ctla2a and Col1a1; c-2 expresses Cxcl13, Gpx3, and Fmo2; c-3 expresses Prlr, Serpine2, and Pappa2; c-4 expresses Ccl11, Apod, and Cxcl2; and c-5 expresses Krt15, Sfn, and Krt14. Among these fibroblast subpopulations, c-1 and c-2 were the major components in both db/db and STZ mice. In contrast, the clustering of fibroblast subpopulations in the skin of diabetic foot patients was more distinct and better defined, with four subclusters: c-1 expressed MMP3, IL24, and COL23A1; c-2 expressed TIMP1, FN1, and INHBA; c-3 expressed GAL, IGFBP5, and CHI3L1; and c-4 expressed

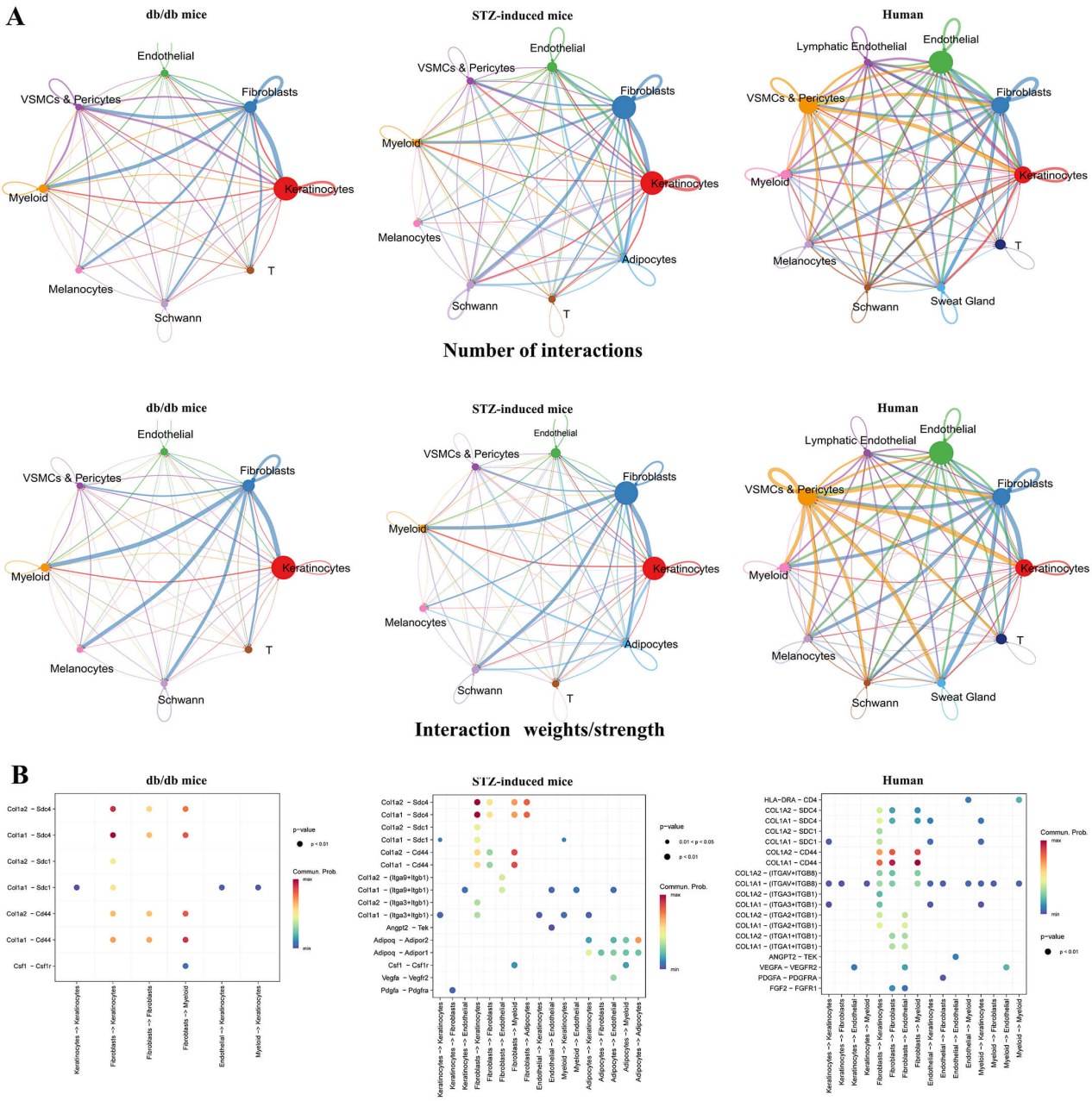


Fig. 3. Cell–cell communication networks. (A) Each node represents a cell population; larger nodes indicate a greater number of cells within that population participating in interactions. Each edge denotes an interaction between the two connected populations; thicker edges indicate stronger interactions, and a greater number of edges connected to a node indicates that the corresponding population engages in more interactions. (B) Ligand–receptor pairs with strong interactions among cell populations.

APOD, RGS6, and AKR1C1. In diabetic foot patients, the c-1 and c-2 subpopulations constituted the majority of the fibroblasts (Fig. 5A,B). Functional enrichment analysis of genes from the most abundant fibroblast subpopulation, c-1, in db/db and STZ mice suggested that this subpopulation played a vital role in extracellular matrix composition (Fig. 5C). The same analysis of the most abundant human fibroblast subpopulation, c-1, demonstrated a strong association with chronic inflammation, matrix remodeling imbalance, and fibrosis (Fig. 5D).

3.8 Differential Analysis of Endothelial Cells

Statistical analysis of differentially expressed genes (DEGs) in endothelial cells from diabetic foot patients compared to db/db mice revealed notable differences. Significantly upregulated skin-related genes in the endothelial cells of diabetic foot patients included CCL2, CD59, HLA-E, COL15A1, CD55, SERPINE1, SOD2, HSPD1, THBS1, and ZEB1. Conversely, significantly downregulated genes included FABP4, SELP, GDF15, CRIP1, APOE, LRG1,

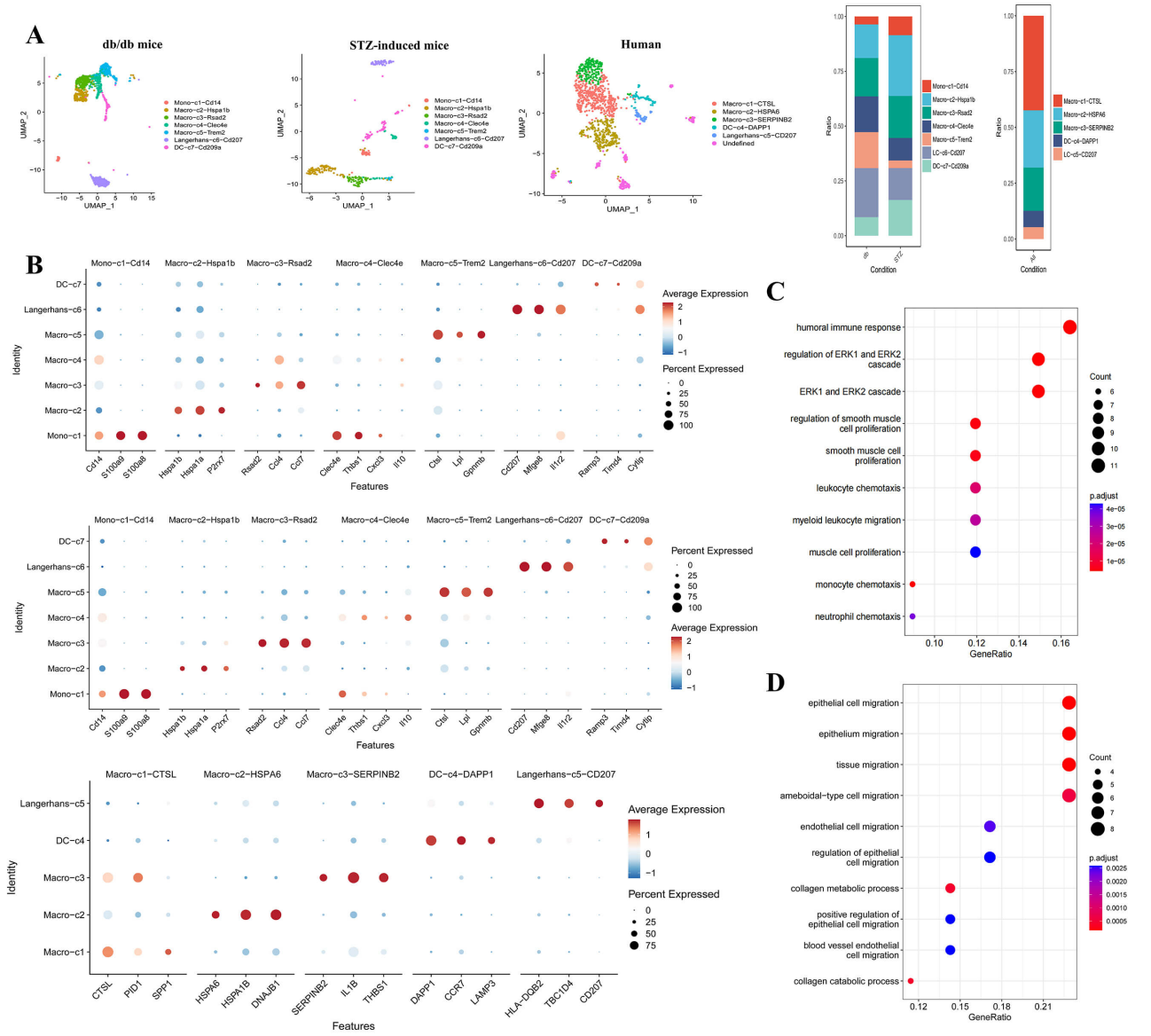


Fig. 4. Myeloid cell subclusters and functional enrichment. (A,B) UMAP and the cell proportions of myeloid subpopulations across groups, and the dot plot of marker gene expression across clusters. (C,D) Functional enrichment analysis of genes from the most abundant myeloid subpopulation in mice and human skin.

EGR1, CD36, LYVE1, and KLF4. GO and KEGG analyses of these DEGs indicated that upregulated genes primarily participated in cell adhesion regulation, wound healing, small GTPase-mediated signal transduction, Ras protein signal transduction, and cellular responses to TGF-β stimuli—functions closely associated with repair, inflammatory responses, and signaling in skin endothelial cells. Downregulated genes were associated mainly with the electron transport chain, mitochondrial ATP synthesis coupled with electron transport, oxidative phosphorylation, cellular respiration, and aerobic respiration, all linked to mitochondrial metabolism and energy production (Fig. 6A).

Similarly, analysis of DEGs in endothelial cells between diabetic foot patients and STZ mice revealed that diabetic foot patients presented significantly upregulated skin-related genes, including CCL2, COL15A1, SOX4, CD59, CD74, SERPINE1, SELE, HLA-E, THBS1, and CD109. Notably, downregulated genes included LYVE1, CEBPB, EGR1, GDF15, CRIP1, APOE, KLF4, JUND, TXNIP, and FTH1. GO and KEGG analyses revealed that the upregulated genes were primarily involved in cell migration, wound healing, epithelial cell proliferation, actin filament organization, and cell-matrix adhesion, all crucial for endothelial cell repair and regeneration. The downregulated genes were mainly related to homotypic cell–cell adhesion, thermoregulation, mechanical stimuli response, adap-

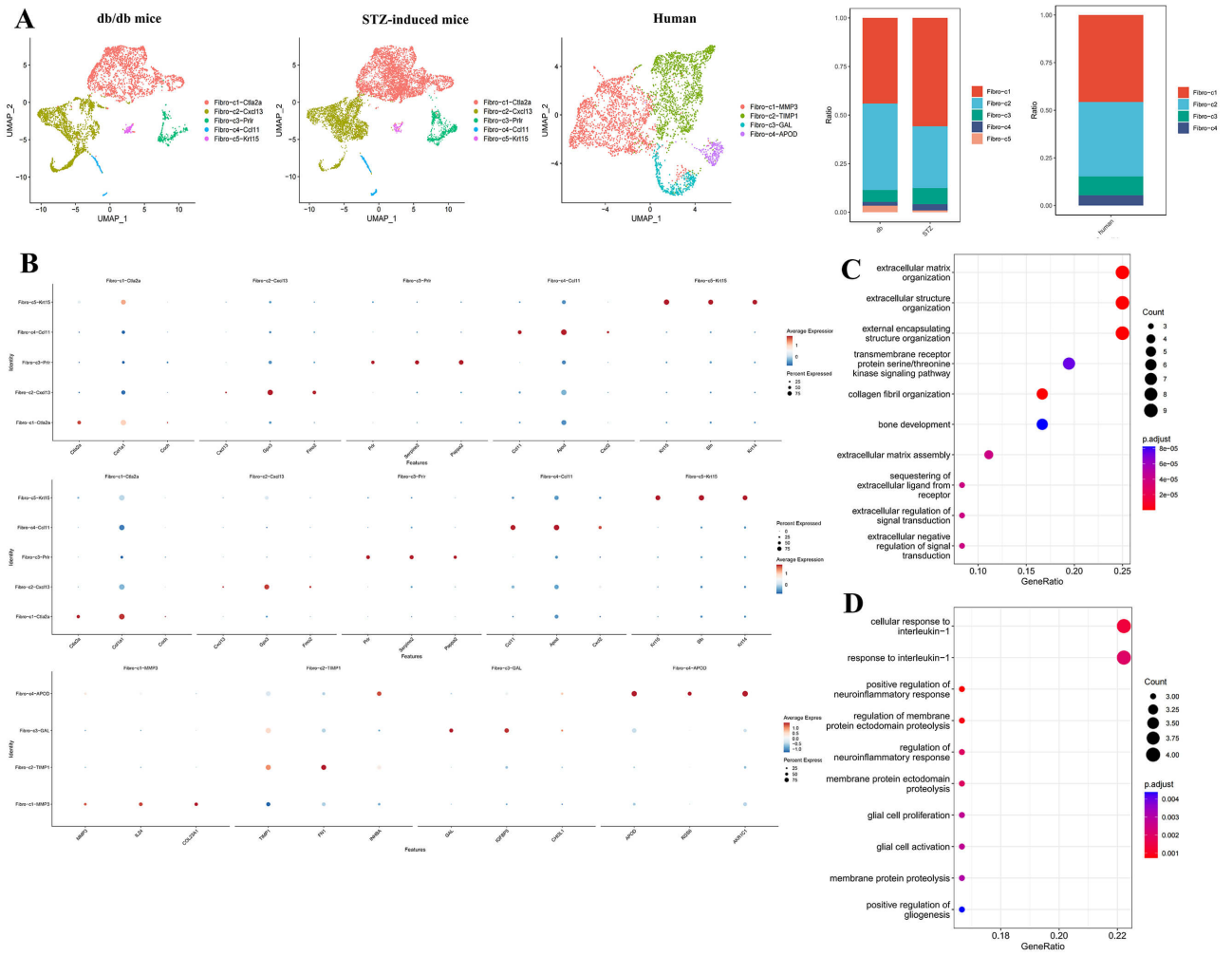


Fig. 5. Fibroblast subclusters and functional enrichment. (A,B) UMAP and the cell proportions of fibroblast subpopulations across groups, and the dot plot of marker gene expression across clusters. (C,D) Functional enrichment analysis of genes from the most abundant fibroblast subpopulation in mice and human skin.

tive thermogenesis, and negative regulation of phosphate metabolic processes, primarily linked to metabolic activity and tissue stability in skin cells (Fig. 6B).

3.9 Differential Analysis of Keratinocytes

Analysis of DEGs in skin keratinocytes between diabetic foot patients and db/db mice revealed critical differences. The significantly upregulated genes in the keratinocytes of diabetic foot patients included S100A8, S100A9, KRT6B, DSC2, SERPINB4, SERPINB3, CD55, SOX4, IL36G, SOD2, ANXA1, PLAUR, NAMPT, GADD45A, and SERPINB13. The significantly downregulated genes comprised CST6, LGALS7B, APOE, SPRR1A, KRT15, KRT79, EPCAM, EGR1, KRT77, ATF3, SCD, CRIP1, BTG2, SDC4, FOS, and CDKN1A. GO analysis revealed that the upregulated genes primarily contributed to wound healing, positive regulation of proteolysis, cellular response to chemical stress, and protein stabilization—all pertinent to skin wound healing, protein stability, and stress response. Conversely, the downregulated genes correlated with the aerobic electron transport chain, ATP synthesis coupled with electron transport, oxidative phosphorylation, and aerobic respiration, linking them to the metabolic activity and energy production capacity of skin keratinocytes (Fig. 6C).

Compared with keratinocytes from STZ mice, keratinocytes from diabetic foot patients showed significant upregulation of S100A8, S100A9, KRT6B, DSC2, SLPI, PLAUR, SERPINB4, SERPINB3, GSTP1, IL36G, SOD2, CD55, GADD45A, CD59, and IL1RN, whereas APOE, KRT15, LGALS7B, CST6, FOS, EGR1, PLET1, EPCAM, IFRD1, SDC4, GSN, SPRR1A, KRT79, and KRT77 were significantly downregulated. GO analysis revealed that the upregulated genes were primarily involved in wound healing, epithelial cell proliferation, peptidase activity regulation, epidermal development, epidermal cell differentiation, and skin barrier establishment—functions key to keratinocyte repair, skin barrier maintenance, and wound heal-

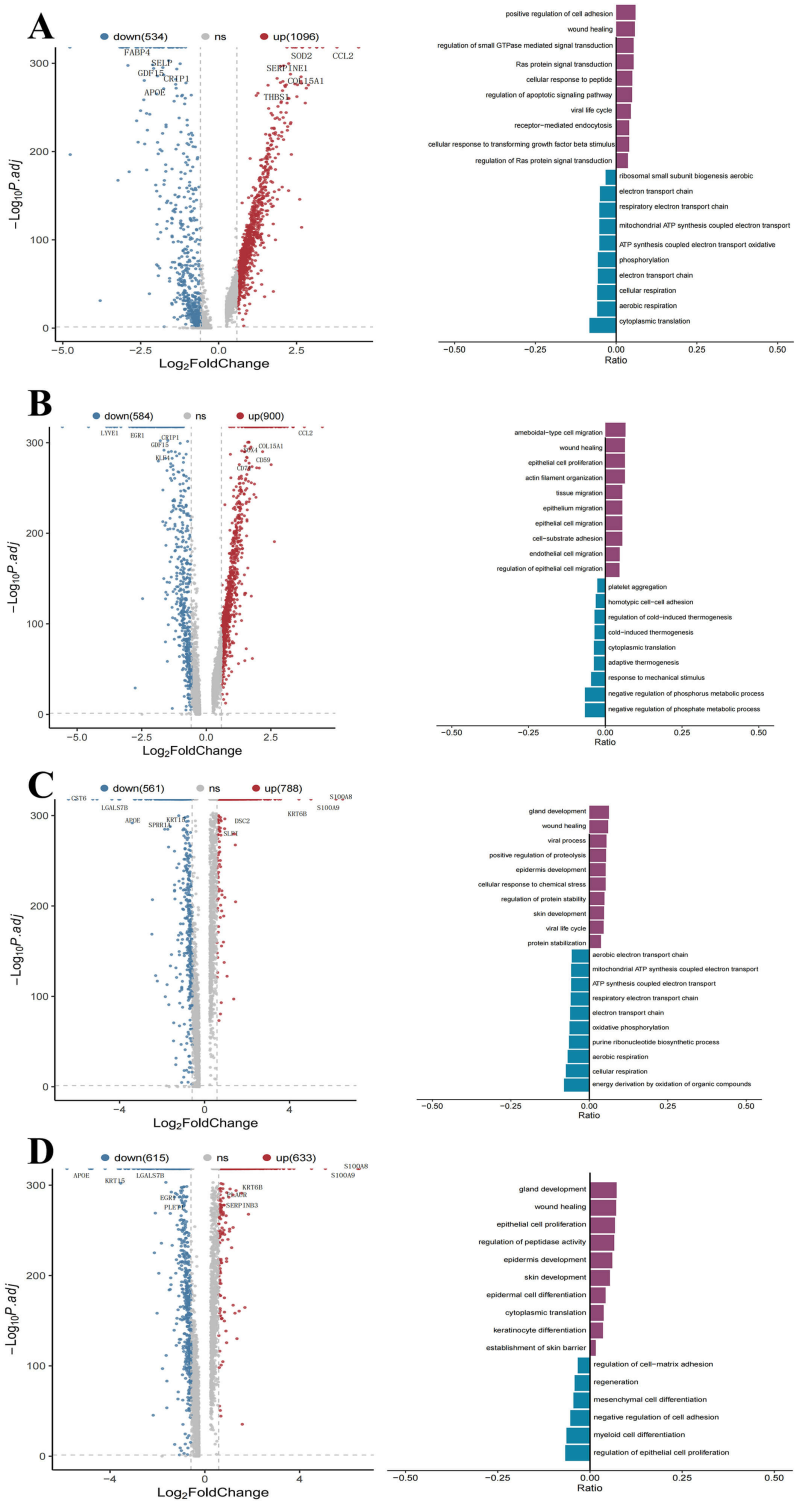


Fig. 6. Endothelial cell differential analysis and keratinocyte differential analysis. (A) Expression profiles of differentially expressed genes between humans and db/db mice in endothelial cells, and the cross-species functional enrichment analyses. (B) Expression profiles of differentially expressed genes between humans and STZ mice in endothelial cells, and the cross-species functional enrichment analyses. (C) Expression profiles of differentially expressed genes between humans and db/db mice in keratinocyte cells, and the cross-species functional enrichment analyses. (D) Expression profiles of differentially expressed genes between humans and STZ mice in keratinocyte cells, and the cross-species functional enrichment analyses. DEGs were identified using $|\log_2$ fold change$| \geq 0.25$ and an adjusted p-value < 0.05.

ing. Meanwhile, the downregulated genes were chiefly associated with the regulation of cell-matrix adhesion, regeneration, mesenchymal cell differentiation, myeloid cell differentiation, and epithelial cell proliferation, reflecting their impact on skin tissue stability and repair capacity (Fig. 6D).

4. Discussion

This study systematically compared the skin characteristics of db/db mice, STZ mice, and diabetic foot patients using single-cell RNA sequencing and pathological analysis. We found that, while similarities exist in tissue composition, there is significant heterogeneity in skin thickness, appendage density, cell cycle dynamics, and intercellular communication networks. Overall, the db/db model more closely mimics the chronic inflammation, skin barrier dysfunction, and metabolic dysregulation observed in humans, which makes it suitable for chronic wound repair research. Conversely, the STZ model, characterized by pronounced stress-response gene expression, is better suited for investigating acute inflammatory responses and early wound healing mechanisms. These findings provide a crucial theoretical basis for selecting appropriate animal models for diabetic skin pathology research.

Significant disparities were observed in tissue morphology and cell proliferation capacity, which are fundamentally attributable to inherent biological differences between species [12]. Furthermore, the paucity of well-structured skin appendages (hair follicles, sebaceous glands, and sweat glands) in human diabetic foot samples warrants careful interpretation. While mice possess dense hair follicles as a species-specific trait, the near-complete absence of appendages in human diabetic foot skin likely reflects a combination of chronic diabetic microangiopathy, tissue fibrosis, and ischemic damage rather than a simple inter-species difference. The reduction of sweat glands, in particular, may contribute to impaired thermoregulation and skin barrier dysfunction in the diabetic foot. At single-cell resolution, the divergent dermal vascular densities and sweat-gland configurations are associated with the chronic hyperglycemic milieu and sustained cutaneous inflammation characteristic of diabetic-foot disease [13,14]. On the other hand, the unique subcutaneous adipose architecture of db/db mice is a direct consequence of their monogenic obesity trait [15,16]. In diabetic-foot skin, the relative expansion of endothelial cells and mural cells (vascular smooth-muscle cells/pericytes) reflects a compensatory, albeit dysregulated, angiogenic response that aligns with the histopathological signature of chronic inflammation, a process increasingly recognized as a target for modulating wound healing [17]. Conversely, the underrepresentation of keratinocytes and fibroblasts is congruent with the compromised regenerative capacity documented in diabetic-foot ulcers [18]. Intriguingly, the paradoxical coexistence of epidermal hyperplasia on histopathology and the paucity of keratinocytes in single-cell suspensions suggests either a cell-autonomous proliferative defect or an increased fragility of diabetic keratinocytes during tissue dissociation, a phenomenon previously reported in diabetic skin [19]. Single-cell analysis revealed that skin cells in diabetic foot patients are predominantly arrested in the G1 phase at the whole-tissue level and fail to effectively progress to the S phase, likely due to hyperglycemia-induced oxidative stress; this reflects a severely limited repair capacity [20]. However, this global observation should be interpreted with caution, as cell cycle distribution likely varies across different cell types. For example, the proliferative status of fibroblasts may differ substantially from that of endothelial cells or keratinocytes, and the G1-phase predominance could therefore be driven by specific subpopulations rather than by pan-cellular arrest. Subgroup cell-cycle analysis by individual cell types is warranted in future studies to dissect the cell-type-specific proliferative defects in diabetic skin. By contrast, both mouse models, particularly STZ mice, showed higher proportions of S- and G2-phase cells, indicating a robust regenerative capacity consistent with an acute stress response rather than the delayed healing phenotype of human diabetic foot ulcers; this contrast highlights the impaired regenerative programs in human DFU, where fibroblast dysfunction and altered ECM remodeling are prominent features [21], and implicates cell-cycle checkpoint dysregulation within diabetic-foot skin as a pivotal driver of the protracted wound healing characteristic of chronic diabetic ulcers [22].

Analysis of intercellular communication and the immune microenvironment revealed distinct regulatory networks. Diabetic foot skin displayed complex cell-cell interactions, particularly between endothelial and inflammatory cells (*HLA-DRA-CD4* signaling), which may contribute to disease progression [23]. Conversely, communication in mouse models was dominated by adipose-derived metabolic signals. Within the myeloid lineage, macrophages were the predominant population across all groups. Notably, db/db macrophages highly expressed chemotactic and anti-inflammatory genes (*Ccl4* and *Il10*), suggesting an immune profile characterized by chronic inflammation and repair that aligns with human pathology [3,24,25]. STZ mice, however, were enriched with monocytes/macrophages high in *S100a8* and *S100a9*, reflecting an acute inflammatory and immune-activated state [26]. By contrast, the skin of diabetic foot patients exhibited a more pronounced chronic inflammatory response and tissue repair activation [27,28,29].

Gene expression profiling of specific cell subpopulations highlighted functional divergences. In fibroblasts, a specific subpopulation expressing *MMP3* and *IL24* was prominent in patients but absent in mice, underscoring the limitations of animal models in replicating human chronic tissue remodeling [30,31,32]. Endothelial cells in patients showed dysregulation of inflammation-related genes (*CCL2*) but downregulation of metabolic markers (*FABP4*

and *KLF4*), suggesting that impaired energy metabolism compromises repair [33]. Similarly, patient keratinocytes exhibited upregulated genes, which play pivotal roles in inflammatory response, immune regulation, and wound repair (*S100A8*, *S100A9*, *SERPINB4*, *SERPINB3*, *SLPI*, and *IL36G*), suggesting that keratinocytes from diabetic foot patients are more actively engaged in maintaining skin barrier function and modulating inflammation [34,35,36,37]. However, the downregulated stemness markers (*CST6*, *KRT15*, *EGR1*, and *FOS*), which are essential for epidermal barrier maintenance and cutaneous repair, imply that keratinocytes in diabetic-foot skin reside in a functionally compromised state [38,39]. Interestingly, keratinocytes in db/db mice shared metabolic pathway alterations (electron transport chain) with human samples, indicating that db/db keratinocytes may hold potential utility for studying mitochondrial dysfunction.

5. Limitations

We acknowledge several limitations of this study. First, the sampling sites differed—dorsal skin for mice versus dorsal foot skin for patients. This mismatch was practically unavoidable but may influence comparability. Mouse dorsal skin and human foot skin differ substantially in epidermal thickness, hair follicle density, vascular distribution, and mechanical loading, factors that may confound cross-species comparisons of cellular composition and gene expression. For instance, the higher vascular density observed in human foot skin may partly reflect the greater mechanical and metabolic demands of the weight-bearing plantar surface, not diabetes-specific pathology alone. This anatomical mismatch should be carefully weighed when interpreting species-specific differences. Second, the small sample size (n = 2 per group for scRNA-seq) limits both the statistical power and the generalizability of our findings. Because the inherent biological variability among human subjects and individual animals may not be fully captured, the observed transcriptional differences should be interpreted with caution. Future studies with larger cohorts and validation using publicly available single-cell datasets are warranted to confirm and extend these observations. Furthermore, neither mouse model fully replicates the prolonged duration of hyperglycemia or the complex chronic inflammatory state of human diabetic foot disease. Finally, as this study relied primarily on sequencing data, future research should incorporate histological validation techniques, such as immunohistochemistry and immunofluorescence, to confirm these findings, thereby establishing a more comprehensive cross-species model comparison.

6. Conclusions

The skin of db/db mice, STZ mice, and diabetic foot patients shows certain similarities in tissue structure and cellular composition, yet there is significant heterogeneity in skin structure thickness, appendage density, the number of cell populations, the cell cycle, cell communication, and the composition and function of specific cell subpopulations. In the skin of diabetic foot patients, genes associated with inflammation and cellular dysfunction are significantly enriched, indicating the presence of an inflammatory state, skin barrier dysfunction, and impaired cellular function; in db/db mouse skin, metabolism-related genes are significantly enriched, suggesting a state of pronounced metabolic dysregulation. In STZ mouse skin, stress-related genes are markedly enriched, indicating a stress-responsive state. Therefore, based on single-cell RNA sequencing, the db/db mouse model is better suited for studies on chronic inflammation, skin barrier dysfunction, chronic wound repair, and energy metabolism disorders in diabetic skin. By contrast, the STZ mouse model is more appropriate for research on acute inflammatory responses, early wound healing, and stress responses in diabetic skin.

Abbreviations

STZ, streptozotocin; ECM, extracellular matrix; HLA, human leukocyte antigen; CCL, C-C motif chemokine ligand; CXCL, C-X-C motif chemokine ligand; IL, interleukin; ADIPOQ, adiponectin; ADIPOR, adiponectin receptor; LEP, leptin; LEPR, leptin receptor; CSF, colony stimulating factor; CSFR, colony stimulating factor receptor; COL, collagen; ITGA, integrin subunit alpha; ITGB, integrin subunit beta; PDGF, platelet-derived growth factor; PDGFR, platelet-derived growth factor receptor; FGF, fibroblast growth factor; FGFR, fibroblast growth factor receptor; MMP, matrix metallopeptidase; TIMP, tissue inhibitor of metalloproteinases; FN, fibronectin; INHBA, inhibin subunit beta A; GAL, galanin; IGFBP, insulin-like growth factor binding protein; CHI3L1, chitinase-3-like protein 1; APOD, apolipoprotein D; RGS, regulator of G protein signaling; AKR1C1, aldo-keto reductase family 1 member C1; SERPINE, serpin family E member; KLF, Krüppel-like factor; EGR, early growth response; FABP, fatty acid binding protein; APO, apolipoprotein; LYVE, lymphatic vessel endothelial hyaluronan receptor; SLPI, secretory leukocyte peptidase inhibitor; CST, cystatin; KRT, keratin; FOS, Fos proto-oncogene.

Availability of Data and Materials

The single-cell RNA-seq data generated in this study have been deposited in the NCBI GEO database: GSE342982 (https://www.ncbi.nlm.nih.gov/geo/query/acc.cgi?acc=GSE342982). The other datasets used or analyzed during the current study are available from the corresponding authors upon reasonable request.

Author Contributions

ZX and RPC contributed equally to this article, ZX designed the study, participated in data analysis and drafted

the manuscript; RPC created the figures and participated in manuscript revision; YFC collected diabetic foot samples, analyzed the pathological data and reviewed the manuscript; YLW analyzed the single-cell sequencing data; ZC collected mouse samples, involved in the construction of mouse models, revised the figures and the manuscript. YBP and YCH conceived the study, secured funding and approved the final manuscript. All authors contributed to editorial changes in the manuscript. All authors read and approved the final manuscript. All authors have participated sufficiently in the work and agreed to be accountable for all aspects of the work.

Ethics Approval and Consent to Participate

The study was approved by the Ethics Committee of Peking University Shenzhen Hospital (No. 2024-122-R2), and all participants provided written informed consent. The study was carried out in accordance with the guidelines of the Declaration of Helsinki. The animal experiments were approved by the Ethics Committee of Peking University Shenzhen Hospital (No. PKUSZH-Ethics-Research-2024-105). All animal procedures were conducted in accordance with the ARRIVE guidelines for the reporting of animal research. The study was performed in compliance with the national guidelines of China, including the Guidelines for the Care and Use of Laboratory Animals (GB/T 35892-2018).

Acknowledgment

The authors thank Dr Qi-Ru Su for the design of the clinical study.

Funding

This research was supported by the Shenzhen Science and Technology Programs (No. GJHZ20210705142543019) and the Shenzhen Medical Research Fund (A2502042).

Conflicts of Interest

The authors declare no conflicts of interest.

Declaration of AI and AI-Assisted Technologies in the Writing Process

During the preparation of this work, the authors used ChatGPT-5.0 in order to check spelling and grammar. After using this tool, the authors reviewed and edited the content as needed and take full responsibility for the content of the publication.

Supplementary Material

Supplementary material associated with this article can be found, in the online version, at https://doi.org/10.31083/FBL50943.

References

[1] Jeffcoate W, Boyko EJ, Game F, Cowled P, Senneville E, Fitridge R. Causes, prevention, and management of diabetes-related foot ulcers. The Lancet. Diabetes & Endocrinology. 2024; 12: 472–482. https://doi.org/10.1016/S2213-8587(24)00110-4

[2] Brooks-Worrell BM, Palmer JP. Setting the Stage for Islet Autoimmunity in Type 2 Diabetes: Obesity-Associated Chronic Systemic Inflammation and Endoplasmic Reticulum (ER) Stress. Diabetes Care. 2019; 42: 2338–2346. https://doi.org/10.2337/dc19-0475

[3] King AJF. The use of animal models in diabetes research. British Journal of Pharmacology. 2012; 166: 877–894. https://doi.org/10.1111/j.1476-5381.2012.01911.x

[4] Renner S, Dobenecker B, Blutke A, Zöls S, Wanke R, Ritzmann M, et al. Comparative aspects of rodent and nonrodent animal models for mechanistic and translational diabetes research. Theriogenology. 2016; 86: 406–421. https://doi.org/10.1016/j.theriogenology.2016.04.055

[5] Avci P, Sadasivam M, Gupta A, De Melo WC, Huang YY, Yin R, et al. Animal models of skin disease for drug discovery. Expert Opinion on Drug Discovery. 2013; 8: 331–355. https://doi.org/10.1517/17460441.2013.761202

[6] Sun Z, Liu Y, Zhao Y, Xu Y. Animal Models of Type 2 Diabetes Complications: A Review. Endocrine Research. 2024; 49: 46–58. https://doi.org/10.1080/07435800.2023.2278049

[7] Um J, Jung N, Kim D, Choi S, Lee SH, Son Y, et al. Substance P preserves pancreatic β-cells in type 1 and type 2 diabetic mice. Biochemical and Biophysical Research Communications. 2018; 499: 960–966. https://doi.org/10.1016/j.bbrc.2018.04.028

[8] Wang YW, Sun GD, Sun J, Liu SJ, Wang J, Xu XH, et al. Spontaneous type 2 diabetic rodent models. Journal of Diabetes Research. 2013; 2013: 401723. https://doi.org/10.1155/2013/401723

[9] Cyr-Depauw C, Cook DP, Mižik I, Lesage F, Vadivel A, Renesme L, et al. Single-Cell RNA Sequencing Reveals Repair Features of Human Umbilical Cord Mesenchymal Stromal Cells. American Journal of Respiratory and Critical Care Medicine. 2024; 210: 814–827. https://doi.org/10.1164/rccm.202310-1975OC

[10] Armand EJ, Li J, Xie F, Luo C, Mukamel EA. Single-Cell Sequencing of Brain Cell Transcriptomes and Epigenomes. Neuron. 2021; 109: 11–26. https://doi.org/10.1016/j.neuron.2020.12.010

[11] Maynard AG, Bhardwaj R, Jones TR, Claussnitzer M. Bridging the variant-to-function gap in type 2 diabetes: advances and challenges. Diabetologia. 2025; 69: 274–294. https://doi.org/10.1007/s00125-025-06600-6

[12] Iismaa SE, Kaidonis X, Nicks AM, Bogush N, Kikuchi K, Naqvi N, et al. Comparative regenerative mechanisms across different mammalian tissues. NPJ Regenerative Medicine. 2018; 3: 6. https://doi.org/10.1038/s41536-018-0044-5

[13] Worsley AL, Lui DH, Ntow-Boahene W, Song W, Good L, Tsui J. The importance of inflammation control for the treatment of chronic diabetic wounds. International Wound Journal. 2023; 20: 2346–2359. https://doi.org/10.1111/iwj.14048

[14] Raja JM, Maturana MA, Kayali S, Khouzam A, Efeovbokhan N. Diabetic foot ulcer: A comprehensive review of pathophysiology and management modalities. World Journal of Clinical Cases. 2023; 11: 1684–1693. https://doi.org/10.12998/wjcc.v11.i8.1684

[15] Singh R, Gholipourmalekabadi M, Shafikhani SH. Animal models for type 1 and type 2 diabetes: advantages and limitations. Frontiers in Endocrinology. 2024; 15: 1359685. https://doi.org/10.3389/fendo.2024.1359685

[16] Emont MP, Jacobs C, Essene AL, Pant D, Tenen D, Colleluori G, et al. A single-cell atlas of human and mouse white adipose tissue. Nature. 2022; 603: 926–933. https://doi.org/10.1038/s41586-022-04518-2
[17] Ghebrehiwet-Kuflom J, Mehta A, Lim P, Dahle S, Isseroff RR. GLP-1 receptor agonists as emerging modulators of inflammation and angiogenesis in chronic cutaneous wound healing. Journal of Investigative Dermatology. 2025; 145: 2981–2988. https://doi.org/10.1016/j.jid.2025.08.045
[18] Voza FA, Huerta CT, Le N, Shao H, Ribieras A, Ortiz Y, et al. Fibroblasts in Diabetic Foot Ulcers. International Journal of Molecular Sciences. 2024; 25: 2172. https://doi.org/10.3390/ijms25042172
[19] Hosseini Mansoub N. The role of keratinocyte function on the defected diabetic wound healing. International Journal of Burns and Trauma. 2021; 11: 430–441.
[20] Cui S, Liu X, Liu Y, Hu W, Ma K, Huang Q, et al. Autophagosomes Defeat Ferroptosis by Decreasing Generation and Increasing Discharge of Free Fe^{2+} in Skin Repair Cells to Accelerate Diabetic Wound Healing. Advanced Science (Weinheim, Baden-Wurttemberg, Germany). 2023; 10: e2300414. https://doi.org/10.1002/advs.202300414
[21] Li X, He Z, Long C, Chen M, Zhang L, Luo Z, et al. Single-Cell Dissection of Fibroblast Heterogeneity in Diabetic Ulcers: Platelet-Rich Plasma (PRP) Therapy Activates Core Regenerative Programs via PLAGL1/RUNX2/ZKSCAN7 Networks. Frontiers in Bioscience (Landmark Edition). 2025; 30: 47450. https://doi.org/10.31083/FBL47450
[22] Zeng JP, Bi B, Chen L, Yang P, Guo Y, Zhou YQ, et al. Repeated exposure of mouse dermal fibroblasts at a sub-cytotoxic dose of UVB leads to premature senescence: a robust model of cellular photoaging. Journal of Dermatological Science. 2014; 73: 49–56. https://doi.org/10.1016/j.jdermsci.2013.08.013
[23] Davis FM, Kimball A, Boniakowski A, Gallagher K. Dysfunctional Wound Healing in Diabetic Foot Ulcers: New Crossroads. Current Diabetes Reports. 2018; 18: 2. https://doi.org/10.1007/s11892-018-0970-z
[24] Reddy MA, Chen Z, Park JT, Wang M, Lanting L, Zhang Q, et al. Regulation of inflammatory phenotype in macrophages by a diabetes-induced long noncoding RNA. Diabetes. 2014; 63: 4249–4261. https://doi.org/10.2337/db14-0298
[25] Seitz O, Schürmann C, Hermes N, Müller E, Pfeilschifter J, Frank S, et al. Wound healing in mice with high-fat diet- or ob gene-induced diabetes-obesity syndromes: a comparative study. Experimental Diabetes Research. 2011; 2010: 476969. https://doi.org/10.1155/2010/476969
[26] Koh TJ, DiPietro LA. Inflammation and wound healing: the role of the macrophage. Expert Reviews in Molecular Medicine. 2011; 13: e23. https://doi.org/10.1017/S1462399411001943
[27] Ginhoux F, Guilliams M. Tissue-Resident Macrophage Ontogeny and Homeostasis. Immunity. 2016; 44: 439–449. https://doi.org/10.1016/j.immuni.2016.02.024
[28] Barman PK, Koh TJ. Macrophage Dysregulation and Impaired Skin Wound Healing in Diabetes. Frontiers in Cell and Developmental Biology. 2020; 8: 528. https://doi.org/10.3389/fcell.2020.00528
[29] Hotamisligil GS. Inflammation and metabolic disorders. Nature. 2006; 444: 860–867. https://doi.org/10.1038/nature05485
[30] Mitamura Y, Nunomura S, Nanri Y, Ogawa M, Yoshihara T, Masuoka M, et al. The IL-13/periostin/IL-24 pathway causes epidermal barrier dysfunction in allergic skin inflammation. Allergy. 2018; 73: 1881–1891. https://doi.org/10.1111/all.13437
[31] Cooper PO, Haas MR, Noonepalle SKR, Shook BA. Dermal Drivers of Injury-Induced Inflammation: Contribution of Adipocytes and Fibroblasts. International Journal of Molecular Sciences. 2021; 22: 1933. https://doi.org/10.3390/ijms22041933
[32] Gimeno-LLuch I, Benito-Jardón M, Guerrero-Barberà G, Burday N, Costell M. The Role of the Fibronectin Synergy Site for Skin Wound Healing. Cells. 2022; 11: 2100. https://doi.org/10.3390/cells11132100
[33] Ishida Y, Kuninaka Y, Nosaka M, Furuta M, Kimura A, Taruya A, et al. CCL2-Mediated Reversal of Impaired Skin Wound Healing in Diabetic Mice by Normalization of Neovascularization and Collagen Accumulation. The Journal of Investigative Dermatology. 2019; 139: 2517–2527.e5. https://doi.org/10.1016/j.jid.2019.05.022
[34] Wang S, Song R, Wang Z, Jing Z, Wang S, Ma J. S100A8/A9 in Inflammation. Frontiers in Immunology. 2018; 9: 1298. https://doi.org/10.3389/fimmu.2018.01298
[35] Boutet MA, Nerviani A, Pitzalis C. IL-36, IL-37, and IL-38 Cytokines in Skin and Joint Inflammation: A Comprehensive Review of Their Therapeutic Potential. International Journal of Molecular Sciences. 2019; 20: 1257. https://doi.org/10.3390/ijms20061257
[36] Sachen KL, Arnold Greving CN, Towne JE. Role of IL-36 cytokines in psoriasis and other inflammatory skin conditions. Cytokine. 2022; 156: 155897. https://doi.org/10.1016/j.cyto.2022.155897
[37] Hovhannisyan Z, Liu N, Khalil-Aguero S, Panea C, VanValkenburgh J, Zhang R, et al. Enhanced IL-36R signaling promotes barrier impairment and inflammation in skin and intestine. Science Immunology. 2020; 5: eaax1686. https://doi.org/10.1126/sciimmunol.aax1686
[38] Wang X, Liu J, Chen J, Xu X, Zhong Y, Xu Y, et al. Loss-of-function mutations in CST6 cause dry skin, desquamation and abnormal keratosis without hypotrichosis. Clinical Genetics. 2023; 103: 301–309. https://doi.org/10.1111/cge.14265
[39] Blanpain C, Fuchs E. Epidermal stem cells of the skin. Annual Review of Cell and Developmental Biology. 2006; 22: 339–373. https://doi.org/10.1146/annurev.cellbio.22.010305.104357